Bragg-confining structures with conventional and effective-mass superlattices

D. Indjin,* V. Milanović, and Z. Ikonić
Faculty of Electrical Engineering, University of Belgrade, Bulevar Revolucije 73, 11000 Belgrade, Yugoslavia
(Received 10 July 1995)

The electronic structure of perturbed superlattices is discussed within the effective-mass approximation. Expressions for bound state energies and wave functions in these structures are derived in general form, valid for any symmetric form of the potential and effective-mass modulation. The special case of rectangular superlattices with a perturbation layer is considered in more detail. The influence of the structure parameters on properties of Bragg-confined states is analyzed for both the conventional structures, and those relying on the effective-mass modulation only, the latter being first proposed in this work. It is found that the fulfillment of Bragg conditions does not necessarily lead to optimally localized Bragg-confined states in conventional structures, but it does in effective-mass modulation ones. Peculiarities of bound states crossing the zero energy gaps are also discussed.

I. INTRODUCTION

Ever since the first proposal of semiconductor superlattices (SL),[1] these structures keep on raising a considerable interest in research of both their fundamental properties and of their possible applications. It is well known that the electronic structure of perfect SL's is miniband like, i.e., it has a series of allowed minibands of continuum states separated by minigaps (e.g., Ref. 2). Deviations of the structure from strict periodicity introduce bound (discrete) states, as is known from the early studies of surface terminated bulk crystal by Tamm.[3] However, Tamm states in semiconductor crystals, lying in the band-gap region, proved very difficult for experimental observation, because real surfaces have a more complicated structure than was initially assumed.[3] On the other hand, the Tamm-like states in the superlattice/bulk interface (the analogue of bulk/vacuum interface) have been experimentally observed,[4] following the theoretical studies of their electronic[5–12] and optical[13–15] properties. Other related structures have also been studied, among them the SL with an "artificial" defect, which is a SL with one of its layers (the perturbation layer) intentionally made different from the others. These were first studied by Combescot and Benoit a la Guillaume[16] and Bastard,[17] and the existence of bound states in them was predicted (however, such states were considered to be very difficult for experimental observation). Physically, the occurrence of such states is explained by considering the perturbation layer as a separate quantum well or barrier, possessing its own resonance and (in the case of well only) bound states. Waves penetrating the SL portions of structure get reflected on SL periods, and if the reflections from all the periods happen to interfere constructively in the perturbation layer region, then one gets a localized wave function, corresponding to a bound state. This is a quantum-mechanical analogue to the well-known optical phenomenon appearing in Fabry-Perot resonators with Bragg mirrors,[18] and in the field of semiconductor SL's it has first been discussed in Ref. 19. The effect has recently been experimentally confirmed by Capasso *et al.*,[20] by measuring the absorption in (AlIn)As/(GaIn)As structure in the infrared. This structure, also known as Bragg-confined structure (BCS), has further been studied theoretically and experimentally.[21–25] Bound states appearing in them are quite interesting in that they resemble to the so-called "bound states in continuum" that occur in some specially tailored potentials in quantum mechanics,[26–28] though there is a significant difference between the two: the Bragg-confined states are isolated by finite gaps from the neighboring continuum regions.

In this paper we present the theoretical considerations of bound states in perturbed SL's, taking the general case of the potential and effective-mass modulation described by arbitrary symmetric functions. Expressions are obtained for bound-state energies and their other properties, which are valid beyond the rectangular Kronig-Penney–type structures. We then specialize to Kronig-Penney–type structures, with the rectangular modulation of the potential and the effective mass, i.e., to BCS's mostly studied at present. Two types of these are considered in more detail: the conventional BCS's, where both the potential and the effective mass are modulated, and "effective-mass BCS," where only the effective mass is modulated while the potential is flat. We explore the bound-state properties as they depend on the structure parameters, and also the relation between the Bragg reflection conditions and degree of bound-state wave-functions localization.

II. THEORETICAL CONSIDERATION

A. Perturbed periodic potential, general consideration

Consider a one-dimensional SL structure, symmetric about the origin, with both the potential and the effec-

0163-1829/95/52(23)/16762(10)/$06.00

tive mass having the periodicity d, and with a perturbation 2δ wide, centered at the origin (Fig. 1). Within the envelope function effective-mass approximation the electron motion is described by

$$-\frac{\hbar^2}{2}\frac{d}{dz}\left(\frac{1}{m(z)}\frac{d\Psi}{dz}\right)+U_{\rm eff}(z)\Psi=E\Psi,$$

$$U_{\rm eff}(z)=U(z)+\frac{\hbar^2k_t^2}{2m(z)}, \tag{1}$$

where Ψ is the envelope function, k_t the transverse wave vector, and $U(z)$ and $m(z)$ the position-dependent potential and the effective mass. There is a double degeneracy of electron states here, with two linearly independent solutions of the Schrödinger equation corresponding to any energy E lying within the allowed minibands of the SL. Out of the perturbation region their wave functions may be written in terms of scattering states

$$\Psi_1(z)=\begin{cases} u_k(z)e^{ik_zz}+Ru_{-k}(z)e^{-ik_zz}, & z<-\delta \\ Tu_k(z)e^{ik_zz}, & z>\delta, \end{cases} \tag{2}$$

$$\Psi_2(z)=\begin{cases} Tu_{-k}(z)e^{-ik_zz}, & z<-\delta \\ u_{-k}(z)e^{-ik_zz}+Ru_k(z)e^{ik_zz}, & z>\delta, \end{cases} \tag{3}$$

where $u_k(z)$ is the periodic part of the Bloch function, and k_z is the z component of the wave vector.

To get purely real wave functions we write the transmission and reflection coefficients as[29] $T=e^{i\tau}\cos\phi$ and $R=ie^{i\tau}\sin\phi$, and make simple linear combinations of scattering states as $\Psi_e(z)=\Psi_1(z)+\Psi_2(z)$ and $\Psi_o(z)=\Psi_2(z)-\Psi_1(z)$. Since $u_k(-z)=u_k^*(z)$, $\mathrm{Re}[u_k(-z)]=\mathrm{Re}[u_k(z)]$, and $\mathrm{Im}[u_k(-z)]=-\mathrm{Im}[u_k(z)]$, it is straightforward to show that these two wave functions have definite parity, i.e., $\Psi_e(-z)=\Psi_e(z)$ and $\Psi_o(-z)=-\Psi_o(z)$. That such wave functions could be constructed also follows from the structure symmetry. Their existence enables one to consider only half of the structure, $z>\delta$. Upon the wave-function normalization to $\delta(k_z-k_z')$ (given in the Appendix) we get

$$\Psi_e(z)=\frac{\mathrm{Re}[u_k(z)e^{i(k_zz+\alpha)}]}{\sqrt{\pi U_d}},\quad z>\delta, \tag{4}$$

$$\Psi_o(z)=\frac{\mathrm{Im}[u_k(z)e^{i(k_zz+\beta)}]}{\sqrt{\pi U_d}},\quad z>\delta, \tag{5}$$

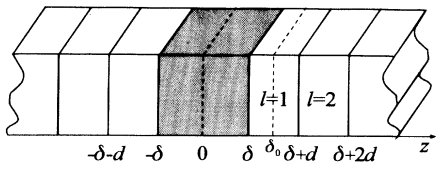

FIG. 1. A schematic representation of a periodic structure with a symmetric perturbation layer centered at the coordinate origin.

where $\alpha=(\tau+\phi)/2$, $\beta=(\tau-\phi)/2$, and $U_d=\frac{1}{d}\int_\delta^{\delta+d}|u_k(z)|^2dz$. The wave function in one period of the SL, say that closest to the origin, may be written as a linear combination of the fundamental solutions of the Schrödinger equation[5,7,30]

$$\Psi(z)=u_k(z)e^{ik_zz}=C[f_e(z)+\theta f_o(z)] \tag{6}$$

Here $f_e(z)$ and $f_o(z)$ denote the functions that are even and odd with respect to the midpoint of that period, $z=\delta_0=\delta+d/2$, due to the symmetry of the potential. These two are obtained by solving the Schrödinger equation, within a SL period, using the fundamental boundary conditions $f_e(\delta_0)=1$, $f_e'(\delta_0)=0$ and $f_o(\delta_0)=0$, $f_o'(\delta_0)=1$. Furthermore, θ is an imaginary constant determined by using Bloch condition $u_k(\delta_0-d/2)=u_k(\delta_0+d/2)$, as

$$\theta=i\left[\frac{f_e(\delta_0+\frac{d}{2})}{f_o(\delta_0+\frac{d}{2})}\right]\tan\left(\frac{k_zd}{2}\right)\equiv i\theta_I, \tag{7}$$

where the term k_zd is found from the miniband dispersion $E(k_z)$, with both the potential and the effective-mass modulation taken into account.[31] In the case we consider, Fig. 1, it reads

$$\cos(k_zd)=\frac{m_{\rm SL}(\delta_0)}{m_{\rm SL}(\delta_0+\frac{d}{2})}[f_e(z)f_o'(z)+f_e'(z)f_o(z)]_{z=\delta_0+\frac{d}{2}}\equiv F(E) \tag{8}$$

where $m_{\rm SL}(z)$ is the position-dependent effective mass. Using Eqs. (4), (5), and (6), the real wave functions of the miniband spectrum inside the lth period $[\delta+(l-1)d<z<\delta+ld]$ may be written as

$$\Psi_e(z)=\frac{1}{U_d}\{[f_e(\tilde z)\cos\alpha-\theta_If_o(\tilde z)\sin\alpha]\cos[(l-1)k_zd]-[f_e(\tilde z)\sin\alpha+\theta_If_o(\tilde z)\cos\alpha]\sin[(l-1)k_zd]\},\quad \delta<\tilde z<\delta+d, \tag{9}$$

$$\Psi_o(z)=\frac{1}{U_d}\{[f_e(\tilde z)\cos\beta-\theta_If_o(\tilde z)\sin\beta]\sin[(l-1)k_zd]+[f_e(\tilde z)\sin\beta+\theta_If_o(\tilde z)\cos\beta]\cos[(l-1)k_zd]\},\quad \delta<\tilde z<\delta+d, \tag{10}$$

where $\overline{U_d} = \frac{\pi}{d}\int_{\delta}^{\delta+d}\left[f_e^2(z) + \theta_I^2 f_o^2(z)\right]dz$ and $\tilde{z} = z - (l-1)d$.

Inside the symmetric perturbation layer the wave functions also have definite parity, and may be written as

$$\Psi_{e,o}(z) = A_{e,o}y_{e,o}(z), \quad -\delta \le z \le \delta, \tag{11}$$

where $y_{e,o}(z)$ are found by using the fundamental boundary conditions $y_e(0) = 1$, $y_e'(0) = 0$ and $y_o(0) = 0$, $y_o'(0) = 1$. The constants α, β, A_e, and A_o in Eqs. (9)–(11) are determined by using the conventional boundary conditions [the continuity of $\Psi(z)$ and $\frac{1}{m(z)}\frac{d\Psi(z)}{dz}$] at $z = \delta$, and for even states are given by

$$\tan\alpha = \frac{1}{\theta_I}\left[\frac{f_e(z)y_e'(z) - \frac{m_\delta(z)}{m_{\mathrm{SL}}(z)}f_e'(z)y_e(z)}{f_o(z)y_e'(z) - \frac{m_\delta(z)}{m_{\mathrm{SL}}(z)}f_o'(z)y_e(z)}\right]_{z=\delta},$$

$$A_e = \frac{f_e(\delta) - \theta_I f_o(\delta)\tan\alpha}{\overline{U_d}\,(1+\tan\alpha)^{1/2}\,y_e(\delta)} \tag{12}$$

and those for odd states have the same form as Eq. (12) upon substitution $\tan\alpha \to \cot\beta$, $\theta_I \to -\theta_I$, $y_e \to y_o$, and $y_e' \to y_o'$. Here $m_\delta(z)$ denotes the electron effective mass in the perturbation layer. This completes the construction of even and odd wave functions corresponding to any particular energy lying in the allowed minibands. For the miniband index to appear explicitly in these expression, the $k_z d$ term obtained from Eq. (8) should be written in the extended-zone representation

$$k_z d = (-1)^n \arccos[F(E)] + 2\pi[n - INT(n/2)] \tag{13}$$

where $n = 0, 1, 2, 3, \ldots$ denotes the index of the minigap just below the miniband to which the particular energy belongs.

Next we consider localized, discrete states lying within minigaps of the SL, which appear due to the perturbation. Using the fact that the wave vector k_z is complex valued in minigaps, given by $k_z = \frac{n\pi}{d} + ik_I$ in the nth minigap,[5,7,30] it follows from Eq. (7) that

$$\theta_{bnd} = -\left[\frac{f_e(\delta_0 + \frac{d}{2})}{f_o(\delta_0 + \frac{d}{2})}\right]\left[\tanh\left(\frac{k_I d}{2}\right)\right]^{(-1)^n} \tag{14}$$

and, from Eq. (8)

$$\cosh(k_I d) = (-1)^n F(E). \tag{15}$$

The wave function of a bound state belonging to the nth minigap therefore has the following form in the lth period of a SL:

$$\Psi_{\mathrm{bnd}\ e,o}(z) = C_{e,o}(-1)^{n(l-1)}e^{(l-1)k_I d} \times[f_e(\tilde{z}) + \theta_{\mathrm{bnd}}f_o(\tilde{z})], \quad \delta < \tilde{z} < \delta + d \tag{16}$$

and inside the perturbation layer it is given by

$$\Psi_{\mathrm{bnd}\ e,o}(z) = B_{e,o}y_{e,o}(z), \quad -\delta < z < \delta. \tag{17}$$

Imposing the boundary conditions at $z = \delta$ to the wave functions (16) (with $l = 1$) and (17) results in a homogeneous linear system for C_e and B_e (C_o and B_o) for even (odd) bound states. Nontrivial solutions of those require the corresponding determinants to equal zero, which results in for even bound states,

$$\left[f_e(\delta)y_e'(\delta) - \frac{m_\delta(\delta)}{m_{\mathrm{SL}}(\delta)}f_e'(\delta)y_e(\delta)\right] + \theta_{\mathrm{bnd}}\left[f_o(\delta)y_e'(\delta) - \frac{m_\delta(\delta)}{m_{\mathrm{SL}}(\delta)}f_o'(\delta)y_e(\delta)\right] = 0 \tag{18}$$

and similarly for odd bound states upon the substitution $y_e' \to y_o'$ and $y_e \to y_o$. Upon the wave-function normalization to unity, i.e., $\int_0^{+\infty}|\Psi_{bnd}(z)|^2dz = 1/2$, the constants $C_{e,o}$ are found to be (see Appendix for more details)

$$C_{e,o} = \frac{1}{\sqrt{2}}\left[\frac{Q}{1 - e^{-2k_I d}} + \left(\frac{f_e(\delta) + \theta_{\mathrm{bnd}}f_o(\delta)}{y_{e,o}(\delta)}\right)R_{e,o}\right]^{-\frac{1}{2}}, \tag{19}$$

where $Q = \int_{\delta}^{\delta+d}\left[f_e^2(z) + \theta_{\mathrm{bnd}}^2 f_o^2(z)\right]dz$ and $R_{e,o} = \int_0^{\delta} y_{e,o}^2(z)dz$, and the values of $B_{e,o}$ are then simply obtained from the wave-function continuity. This completes the construction of bound-state wave functions, expressed in terms of the fundamental solutions of the Schrödinger equation. These wave functions decay off the perturbation layer with the decay constant given by Eq. (15).

The electron density in this structure includes contributions from bound and continuum (miniband) states. With each state within the miniband part of the spectrum being double degenerate, the electron density on any single minibands reads[32]

$$n_{i\,\mathrm{con}}(z) = \frac{1}{2\pi^2}\int_0^{+\infty} d(k_t^2)\int_{k_{z\,\min}}^{k_{z\,\max}}(|\Psi_e|^2 + |\Psi_o|^2)f_{\mathrm{FD}}(E, E_F)dk_z, \tag{20}$$

where f_{FD} is the Fermi-Dirac distribution function and E_F the Fermi level. The sum of wave-function moduli squared in (20) may, using Eqs. (4), (5), (6), (9), and (10), be written as

$$|\Psi_e|^2+|\Psi_o|^2=|u_k(\tilde{z})|^2+\frac{2\sin(\beta-\alpha)}{\overline{U_d}^2}\Big\{[f_e^2(\tilde{z})-\theta_I^2 f_o^2(\tilde{z})]\sin[\alpha+\beta+2(l-1)k_z d]$$
$$-\theta_I f_e(\tilde{z})f_0(\tilde{z})\cos[\alpha+\beta+2(l-1)k_z d]\Big\},$$
$$=|u_k(\tilde{z})|^2-|\Delta u_k(\tilde{z})|^2, \qquad \delta<\tilde{z}<\delta+d \tag{21}$$

in the SL part of the structure, and the electron density in the ith miniband then takes the form $n_{i\,\mathrm{con}}(z)=n_{i\,\mathrm{con}}^{\mathrm{ID}}(z)-\Delta n_{i\,\mathrm{con}}(z)$ for $z>\delta$. Here $n_{i\,\mathrm{con}}^{\mathrm{ID}}(z)$ is the electron density in the ith miniband of the ideal (unperturbed) SL, and the excess density $\Delta n_{i\,\mathrm{con}}(z)$, occurring due to the presence of perturbation, the latter one decaying away from the perturbation layer as $1/ld$. The electron density on a bound state is found from

$$n_{j\,\mathrm{bnd}}(z)=\frac{1}{2\pi}\int_0^{+\infty}|\Psi_{j\,\mathrm{bnd}}(z,E_j,k_t^2)|^2\,f_{\mathrm{FD}}(E_j,E_F)\,d(k_t^2) \tag{22}$$

Certainly, the presence of a single perturbation layer in infinite SL does not shift the Fermi level from the position that it takes in the ideal SL, itself determined from the global neutrality.[33]

B. Application to the Kronig-Penney type superlattices: Bragg-confined structures

While the considerations given above apply to SL's with any symmetric potential in their periods, most calculations would have to be done numerically. The special case of rectangular (Kronig-Penney type) SL's, however, allows one to obtain analytic, closed-form expressions. Rectangular modulation of the potential and the effective mass is a good approximation to many real structures of that type, at least for not too large doping levels N_s so that the self-consistency effects can be neglected. The potential in perturbed Kronig-Penney SL, with the perturbation layer made of the quantum-well-type material, is given in Fig. 2.

The even-parity particular solution of the Schrödinger equation in first period of the SL ($\delta_0-\frac{d}{2}<z<\delta_0+\frac{d}{2}$) is

$$f_e(z)=\begin{cases}\cos[k_W(z-\delta_0)], & \delta_0-\frac{a}{2}<z<\delta_0+\frac{a}{2},\\ K_1e^{k_B(z-\delta_0)}+K_2e^{-k_B(z-\delta_0)}; & E<U_{0\mathrm{eff}},\\ K_1'\cos[k_B'(z-\delta_0)]+K_2'\sin[k_B'(z-\delta_0)]; & E>U_{0\mathrm{eff}},\end{cases}\quad \delta_0+\frac{a}{2}<z<\delta_0+\frac{d}{2},$$
$$\begin{cases}K_2e^{k_B(z-\delta_0)}+K_1e^{-k_B(z-\delta_0)}; & E<U_{0\mathrm{eff}},\\ K_1'\cos[k_B'(z-\delta_0)]-K_2'\sin[k_B'(z-\delta_0)]; & E>U_{0\mathrm{eff}},\end{cases}\quad \delta_0-\frac{d}{2}<z<\delta_0-\frac{a}{2}, \tag{23}$$

where $k_W=\sqrt{\frac{2m_W}{\hbar^2}(E-E_{t\,W})}$, $k_B=\sqrt{\frac{2m_B}{\hbar^2}(U_0-E+E_{t\,B})}$, $k_B'=\sqrt{\frac{2m_B}{\hbar^2}(E-U_0-E_{t\,B})}$, and $U_{0\mathrm{eff}}=U_0+E_{t\,B}$ with $E_{t\,W,B}=\frac{\hbar^2k_t^2}{2m_{W,B}}$. The integration constants are found from the continuity of $f_e(z)$ and $\frac{1}{m(z)}f_e'(z)$ at $z=\delta_0+\frac{a}{2}$ as

$$K_{1,2}=\frac{1}{2}e^{\mp\frac{k_Ba}{2}}\left[\cos\left(\frac{k_Wa}{2}\right)\mp\xi\sin\left(\frac{k_Wa}{2}\right)\right],$$
$$K_{1,2}'=\begin{bmatrix}\cos\\ \sin\end{bmatrix}\left(\frac{k_B'a}{2}\right)\cos\left(\frac{k_Wa}{2}\right)\pm\xi'\begin{bmatrix}\sin\\ \cos\end{bmatrix}\left(\frac{k_B'a}{2}\right)\sin\left(\frac{k_Wa}{2}\right), \tag{24}$$

where $\xi=\frac{k_Wm_B}{k_Bm_W}$ and $\xi'=\frac{k_Wm_B}{k_B'm_W}$. The even-parity fundamental solution in the perturbation layer $y_e(z)$ has same form as given in Eqs. (23) and (24) upon the substitution $a\to c$, $d\to 2\delta$, and $\delta_0\to 0$. The corresponding odd-parity solutions $f_o(z)$ and $y_o(z)$ are determined in the same manner, and have analogous forms. Here we have $m_{\mathrm{SL}}(\delta_0)\equiv m_W$ and $m_{\mathrm{SL}}(\delta_0+\frac{d}{2})\equiv m_B$, and the miniband spectrum, Eq. (8), reduces to the well-known form[2,5,17]

$$\cos(k_zd)=\cos(k_Wa)\cos(k_B'b)+\tfrac{1}{2}(\xi'^{-1}-\xi')\sin(k_Wa)\sin(k_B'b),\quad E>U_{0\mathrm{eff}}, \tag{25}$$

while in the case $E<U_{0\mathrm{eff}}$ one substitutes $\sin(k_B'b)\to i\sinh(k_Bb)$, $\cos(k_B'b)\to\cosh(k_Bb)$, with $k_B=ik_B'$. Also, using $m_\delta(\delta)=m_{\mathrm{SL}}(\delta)=m_B$, the normalization constant $\overline{U_d}$ and phase factors α and β, as well the wave functions (9) and (10) may be straightforwardly calculated. Furthermore, the transcendent equation (18) and the corresponding one for odd states, which give the energies of bound states in minigaps, are satisfied when

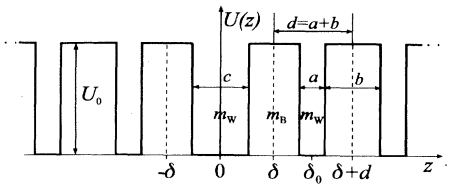

FIG. 2. The conduction-band edge diagram of the Kronig-Penney-type superlattice with the central layer of different width than other corresponding layers.

$$k_W c = q\pi, \quad E > U_{0\text{eff}}, \tag{26}$$

$$\left[\tan\left(\frac{k_W c}{2}\right)\right]^{(-1)^{t+1}} = (-1)^t \xi, \quad E < U_{0\text{eff}}, \tag{27}$$

$$k'_B b = (r + \tfrac{1}{2})\pi, \quad E > U_{0\text{eff}}, \tag{28}$$

$$k_B b = (r + \tfrac{1}{2})\pi, \quad E < U_{0\text{eff}}, \tag{29}$$

$$k_W a = (s + \tfrac{1}{2})\pi, \tag{30}$$

where $(q-1), t, r, s = 0, 1, 2, 3, \ldots$.

Equation (26) actually corresponds to the expression for resonant states above the barrier in a quantum-well structure, and Eq. (27) is the familiar transcendent equation for quantum-well bound states. The next three equations [(28) and (30) for energies above the barrier, and (29) and (30) for energies below the barrier] correspond to quantum-mechanical Bragg reflection conditions. By a suitable choice of SL parameters, therefore, bound and resonant states of the perturbation layer (considered as a quantum well) all become bound states of this structure, with their energies preserved. The most interesting effect here certainly is the localization of resonant states above the barrier, i.e., the appearance of Bragg-confined states. Structures where conditions (26), (28), and (30) are satisfied are also known as Bragg-confined structures.[20–24] They are analogous to the optical Fabry-Pérot resonators with $\lambda/4$-stack Bragg mirrors.[18] Physically the localization is brought about by constructive interference in the perturbation layer of waves reflected quantum mechanically on the array of well-barrier interfaces, similarly as in optics. The analogy is limited, however, with two parameters (the potential and the effective mass) being modulated in BCS, in contrast to just one parameter (the refractive index) in optics.

From Eq. (16) it follows that the degree of localization is determined by the imaginary wave vector k_I, which is largest for energies in the middle of minigaps. Above the barriers this is best fulfilled for the same energies where Bragg conditions are met. Deviation from the exact Bragg conditions shifts the bound-state energy from its optimal position in the minigap, and reduces the degree of localization. States above the barrier, stemming from resonances embedded in continuum, are more sensitive than those below the barrier.

III. NUMERICAL RESULTS AND DISCUSSION

The theory displayed in Sec. II was used for numerical calculations of two types of BCS with Kronig-Penney SL's. The first type is the one based on the $Al_{0.48}In_{0.52}As/Ga_{0.47}In_{0.53}As$ system, used in theoretical and experimental studies by Capasso *et al.*[20–22] The second type is based on $Ga_{0.31}In_{0.69}As/InP$ system, having a flat conduction-band edge but discontinuous effective-mass. It is thus derived from the effective mass SL's proposed some time ago[34–36] and is interesting because it bears the full analogy to the corresponding optical systems. In either case we have taken the band nonparabolicity into account. This is implemented through the frequently used concept of energy-dependent effective mass, based on the two-band Kane model (the details of the scheme are described by Nelson, Miller, and Kleinman[37]). Following this approach the well and barrier effective masses depend on energy as

$$m_W(E) = m_{W0}\left(1 + \frac{E}{E_{gW}}\right),$$
$$m_B(E) = m_{B0}\left(1 - \frac{U_0 - E}{E_{gB}}\right), \tag{31}$$

where m_{W0} and m_{B0} are the conduction-band edge effective masses, E_{gW} and E_{gB} the band gaps, and U_0 the conduction-band offset at interfaces.

In calculations for the (AlIn)As/(GaIn)As SL's the material parameters were taken as $m_{W0} = 0.043m_0$, $E_{gW} = 0.87$ eV for the "well" material $Ga_{0.47}In_{0.53}As$, with the corresponding nonparabolicity parameter $\gamma_W = 1.01 \times 10^{-18}$ m^2 being in good agreement with the data of Ref. 38 and with the values used in Refs. 20–22, and $m_{B0} = 0.073m_0$, $E_{gB} = 1.49$ eV for the "barrier" material $Al_{0.48}In_{0.52}As$. The conduction-band offset between the two is $U_0 = 0.5$ eV. The thickness of the well layers was $a = 16$ Å, and of the barriers $b = 39$ Å, while the perturbation layer, made of the well-type semiconductor, was $c = 2a = 32$ Å wide. This system is found to have one below-the-barrier miniband extending from 306.8 to 387.2 meV, and one above-the-barrier miniband from 640.5 to 880 meV, in the range of energies from the well conduction-band bottom (reference zero) to 1 eV. Due to the perturbation layer there also exist bound states: one even-parity state below the first miniband, at $E_0 = 203.2$ meV, and two odd-parity states in the two minigaps, at $E_1 = 562.7$ meV and $E_2 = 890.3$ meV, both above the barrier top. The energy difference $E_1 - E_0 = 359.5$ meV is in excellent agreement with the experimentally measured absorption peak in this structure,[20,21] and also with the results of the transfer-matrix-based calculation.[24] The structure was designed to provide Bragg confinement of the first state above the barrier, i.e., at $E = E_1$, and the localization fac-

tors of the three bound states are $k_I d = 2.36$ at $E = E_0$, $k_I d = 1.12$ at $E = E_1$, and $k_I d = 0.209$ at $E = E_2$. Upon finding the wave functions, the localization coefficients, defined as $\eta(E_j) = \int_0^\delta |\Psi_{j\,\mathrm{bnd}}|^2 dz / \int_0^{+\infty} |\Psi_{j\,\mathrm{bnd}}|^2 dz$, for the three states are calculated to be $\eta(E_0) = 97.5\%$, $\eta(E_1) = 79.1\%$, and $\eta(E_2) = 17.4\%$. While the lowest bound state is well localized simply because it is deep below the barrier top, it is precisely the Bragg confinement that makes the second state also quite well localized. Interestingly, however, this second state is not optimally positioned (it is not in the middle of minigap) in respect to the degree of localization, although the Bragg conditions are exactly met at $E = E_1$. These conditions are far from being fulfilled at $E = E_2$, which is the real reason (and not simply its high energy) that this state is poorly localized.

The properties of bound states in this structure have been explored as they depend on the structure parameters. In this set of calculations the barrier width was fixed at $b = 39$ Å, and the well width varied from 16 to 65 Å, with a couple of different values of the perturbation layer width c. All these calculations were performed at zero transverse wave vector k_t: due to a large band offset U_0, changing k_t did not have a significant influence on the results. The results are displayed in Fig. 3. The position of even (odd) parity bound states is denoted by solid (dashed) lines, while dotted lines give the optimum position of these states in respect to the degree of localization. Shaded regions correspond to allowed minibands.

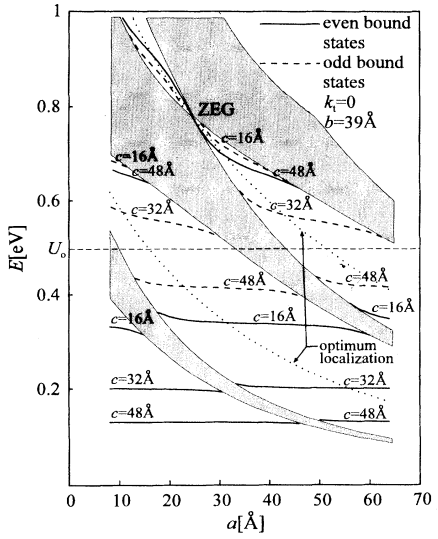

FIG. 3. The miniband structure of (AlIn)As/(GaIn)As superlattice with a perturbation layer, as it depends on the width of well-type layers a, for a couple of values of perturbation layer width c, and for the barrier layers width $b = 39$ Å (at $k_t = 0$). The allowed minibands are shaded, the even-parity bound states are represented by solid lines, and odd-parity ones by dashed lines. Dotted lines denote the position of bound states which would be optimal in respect to the degree of their localization.

One can see that properties of bound states, when deeply below the barrier top, do not depend very strongly on the SL parameters. These states, derived from the "leaky" bound states of the perturbation layer quantum well, are essentially determined from its width c and the barrier height U_0. When a state comes close to the barrier top, it becomes more sensitive to the SL parameter variation, especially if an allowed miniband is nearby. On the other hand, bound states above the barrier, derived from the perturbation layer resonances, are very sensitive to the SL parameters, especially at higher energies.

Also interesting is the behavior of bound states when the structure parameters vary so that zero energy gaps (ZEG) appear (exactly or nearly so). No matter how narrow a minigap is, at least one bound state occurs, with its (their) parity conserved upon crossing the ZEG. Such states bear most resemblance to bound states in continuum discussed in Refs. 26–28. However, the degree of localization, proportional to $k_I d$, diminishes as the minigap gets smaller, and at the exact ZEG condition these states become essentially delocalized. In the example given in Fig. 3 the ZEG condition occurs for $a = 24$ Å in the second minigap, and the bound state crossing it is derived from the first resonant state of the perturbation layer, its width being $c = 2a = 48$ Å, for which we find from Eqs. (26) and (30) with $q = 1$ and $s = 0$ that one of Bragg conditions is fulfilled. As a final note, one can see from Fig. 3 that bound states all disappear in case $a = c$, i.e., when the structure reduces to a perfect SL.

Another set of calculations for this type of structure was performed in the following way. The width of the perturbation layer c was varied in the range 20 – 80 Å, the position of its first resonance state was determined according to $k_W c = \pi$, and then the well and barrier layer widths of the SL, a and b, were fitted to meet the first-order Bragg-confinement conditions $k'_B b = k_W a = \pi/2$ (therefore $a = c/2$). When the width c increased so that the resonant state sank below the barrier top, its energy was determined from the transcendent equation (27), i.e., $\cot(k_W c/2) = -\xi$. The results of these calculations are given in Fig. 4. As c increases the corresponding values of b, given parametrically in the bottom horizontal axis, increase at first slowly, then rather rapidly when the resonance approaches U_0, and finally, when it sinks below U_0 the value of b decreases slowly. Throughout this variation of structure parameters, the energy of the Bragg-confined state coincides with the position of the single quantum-well resonance or bound state (depending on its width c),[2] which simply confirms that the conditions (26)–(30) satisfy Eq. (18) for the Kronig-Penney SL. Along with the position of the Bragg-confined state obtained as described, Fig. 4 also gives its optimal position with respect to the degree of wave function localization. There clearly is some difference between the two, becoming very large when the Bragg-confined state comes close to the barrier top. The reason that any difference appears is, as noted in Sec. II, that both the effective mass and the potential are modulated. Finally, one can again notice from Fig. 4 that the parity of the Bragg-confined state is conserved in crossing the ZEG point induced by variation of the

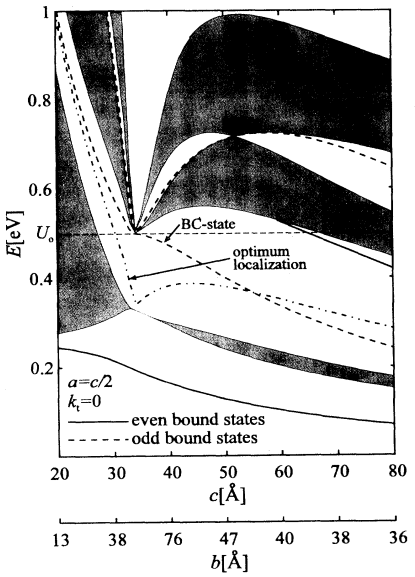

FIG. 4. The miniband structure of (AlIn)As/(GaIn)As Bragg-confined structure, as it depends on the perturbation layer width c. The width of barrier layers b was fitted to meet Bragg conditions for the odd-parity bound state in the first minigap (BC state) and is given on the bottom horizontal axis. The shaded areas denote the allowed minibands.

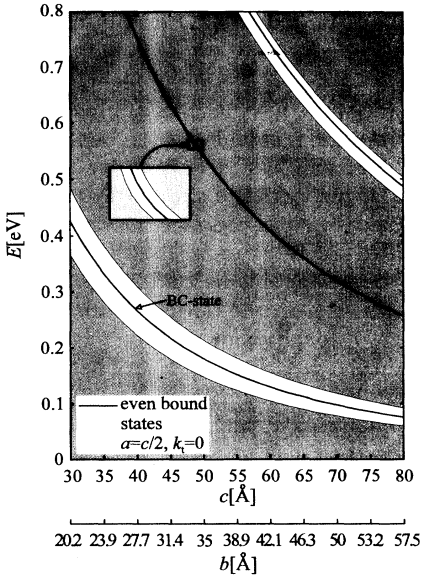

FIG. 5. The miniband structure of (InGa)As/InP effective mass Bragg-confined structure, as it depends on the perturbation layer width c. The width of barrier layers b was fitted to meet Bragg conditions for the even-parity bound state in the first minigap (BC state) and is given on the bottom horizontal axis. The shaded areas denote the allowed minibands.

structure geometrical parameters.

The second type of structure analyzed in this work is the one having the effective-mass modulation only, the potential (i.e., the conduction-band edge) being kept constant. By comparing the time-independent Schrödinger and Helmholtz equation for electromagnetic waves in layered media,[39,40] such a structure is seen to be fully analogous to the optical layered structure, where the effective mass corresponds to the refractive index squared. The BCS of that type is actually an effective-mass SL (EMSL) (Refs. 34 and 35) with just one of its layers made wider than the others, constituting thus an effective mass BCS. Calculations were performed for $Ga_{0.31}In_{0.69}As/InP$-based system.[34,36] The material parameters used for the two semiconductors are $m_{W0} = 0.073m_0, m_{B0} = 0.043m_0, E_{gW} = 1.26$ eV, and $E_{gB} = 0.69$ eV, where the well-barrier notation was kept and assigned to individual materials according to the effective-mass ratio [the semiconductor with the lower effective mass becomes the effective barrier for nonzero k_t (Ref. 36)]. The perturbation layer width c was varied in the range 30–80 Å, and the SL layers widths a and b were fitted to meet Bragg conditions for the first resonant state. The results are displayed in Fig. 5. Here we find an even-parity bound state lying in the middle of the minigap throughout the range of structure parameters explored, having thus the optimal position for the wave-function localization (as is the case in the corresponding optical systems). Previous considerations of perfect EMSL indicated the existence of ZEG conditions for all even-numbered minigaps at $k_t = 0$ in case $m_B b^2 = m_W a^2$, provided the nonparabolicity effects are ignored. One can see from Fig. 5 that taking the nonparabolicity into account induces a very narrow minigap. There is an even-parity bound state embedded in it, caused by the perturbation layer.

Analysis of the EMSL (Ref. 35) also pointed to a strong dependence of their miniband structure on k_t, so we have here also explored the effects of k_t variation on perturbed SL's. Results of an example calculation, with $c = 70$ Å, $a = 35$ Å, $b = 50$ Å, and k_t in the range $0 - 0.1$ Å^{-1} are given in Fig. 6. As k_t varies and ZEG conditions appear at one value or another (regardless of whether induced by nonparabolicity or not), the Bragg-confined states change their parity upon crossing the ZEG. This is in contrast to what happens to them in the case of the structure parameters variation induced ZEG points, the situation discussed above. The effect of parity flipping is quite interesting, in that it would make pairs of states active in optical intersubband transitions only in limited ranges of the transverse wave vector k_t.

Finally, we have made calculations of electron density distribution in (AlIn)As/(GaIn)As and (GaIn)As/InP BCS's, taking the doping density $N_s = 3 \times 10^{11}$ cm^{-2} (this is the volume density integrated in one period of the SL), at $T = 300$ K. The Fermi level in (AlIn)As/(GaIn)As structure as considered by Capasso *et al.*[20,21] ($c = 32$ Å, $a = 16$ Å, $b = 39$ Å) is $E_F = 232$ meV. Electron densities on the lowest two bound states ($n_{0\,\mathrm{bnd}}$ and $n_{1\,\mathrm{bnd}}$) and on the lowest two minibands ($n_{1\,\mathrm{con}}$ and $n_{2\,\mathrm{con}}$) are given in Fig. 7, together with the difference densities ($\Delta n_{1\,\mathrm{con}}$ and $\Delta n_{2\,\mathrm{con}}$) referenced to

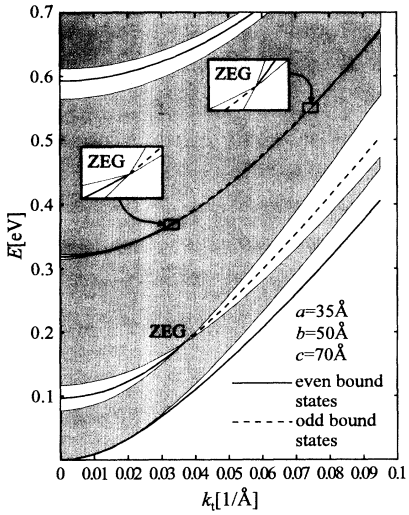

FIG. 6. The miniband structure of (InGa)As/InP effective-mass Bragg-confined structure, as it depends on the transverse wave vector k_t, calculated for a single set of the structure parameters. The shaded areas denote the allowed minibands.

the unperturbed SL case. Calculations for the effective-mass BCS ($c = 70$ Å, $a = 35$ Å, $b = 50$ Å) give $E_F = -7$ meV at $T = 300$ K, and the corresponding electron densities are displayed in Fig. 8. As one can see from Fig. 7, the electron density on the lowest bound state exceeds

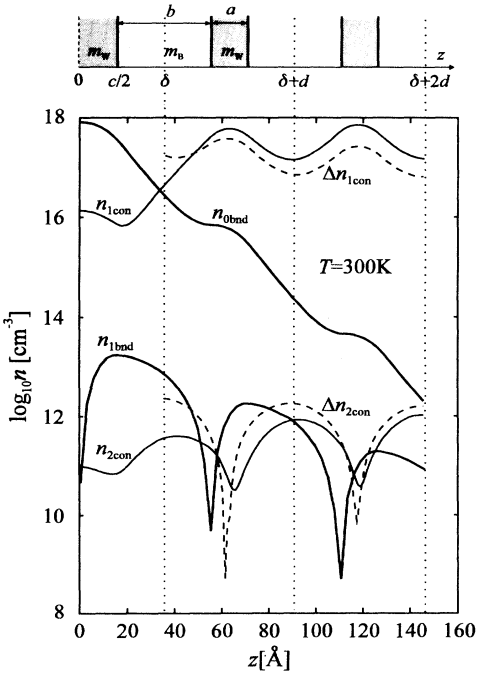

FIG. 7. The electron density profiles for the lowest two minibands ($n_{1\,\mathrm{con}}, n_{2\,\mathrm{con}}$) and the lowest two bound states ($n_{0\,\mathrm{bnd}}, n_{1\,\mathrm{bnd}}$) in (AlIn)As/(GaIn)As Bragg-confined structure. Also given (dashed lines) are the difference densities ($\Delta n_{1\,\mathrm{con}}, \Delta n_{2\,\mathrm{con}}$), referenced to the perfect superlattice case. The structure parameters are $c = 32$ Å, $a = 16$ Å, $b = 39$ Å.

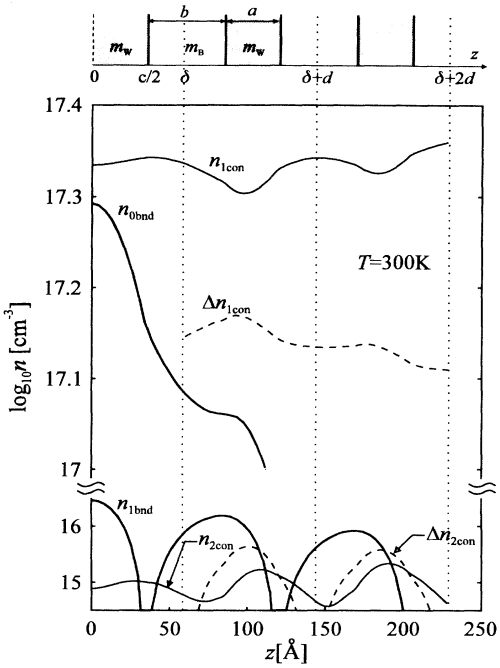

FIG. 8. The electron density profiles for the lowest two minibands ($n_{1\,\mathrm{con}}, n_{2\,\mathrm{con}}$) and the lowest two bound states ($n_{0\,\mathrm{bnd}}, n_{1\,\mathrm{bnd}}$) in (InGa)As/InP effective-mass Bragg-confined structure. Also given (dashed lines) are the difference densities ($\Delta n_{1\,\mathrm{con}}, \Delta n_{2\,\mathrm{con}}$), referenced to the perfect superlattice case. The structure parameters are $c = 70$ Å, $a = 35$ Å, $b = 50$ Å.

the density in minibands by two orders of magnitude at $z = 0$, but the two become comparable at $z = \delta$. The perturbation layer significantly influences the electron density in minibands, as compared to the unperturbed SL case: the difference densities in Fig. 7 show a rather slow decay towards zero. We may also note that a low population of above-the-barrier Bragg-confined state, accompanied by its good localization, should give rise to significant absorption on $E_0 \rightarrow E_1$ transitions. Similar conclusions apply to the effective-mass BCS (Fig. 8), except that the bound-state density overshoot is not so remarkable here.

IV. CONCLUSION

The theory of electronic structure of perturbed SL's was presented, within the framework of the effective-mass approximation. The expressions for bound-state energies in these structures were derived in general form, in terms of the fundamental solutions of the Schrödinger equation. The special case of rectangular SL's with a perturbation layer was then considered in more detail. The influence of the structure parameters on properties of Bragg-confined states was explored for both the conventional BCS and the one based on the effective-mass modulation only, proposed in this work. The latter are found to be fully anal-

ogous to optical BCS's, in the sense that the fulfillment of Bragg conditions gives maximally localized bound states, which is not the case in conventional BCS's. Peculiarities of states crossing the k_t-induced ZEG points were also discussed.

The methods presented are also applicable, directly or upon generalization, to analysis of related structure like a quantum well embedded between two different SL's, or between the bulk semiconductor and SL, etc. Calculations of optical properties of BCS's, based on the methods described here, are under way and will be presented in due course.

APPENDIX

The continuum (miniband) spectrum wave functions are normalized according to

$$\int_{-\infty}^{+\infty} \Psi_{k_z}\Psi^*_{k'_z}dz = \delta(k_z - k'_z), \tag{A1}$$

which, due to definite parity of wave functions, may also be written as

$$2\int_{\delta}^{+\infty} \Psi_{k_z}\Psi^*_{k'_z}dz + 2\int_{0}^{\delta} \Psi_{k_z}\Psi^*_{k'_z}dz = \delta(k_z - k'_z). \tag{A2}$$

The second term in (A2) has a finite value, and may be neglected with respect to the first term. For even-parity states, using Eq. (4), the first term takes the form

$$\begin{aligned} I &= \int_{\delta}^{+\infty} \Psi_{e,k_z}(z)\Psi^*_{e,k'_z}(z)dz \\ &= K_eK'_e\int_{\delta}^{+\infty} \{\mathrm{Re}[u_k(z)]\cos(k_zz+\alpha) - \mathrm{Im}[u_k(z)]\sin(k_zz+\alpha)\} \\ &\quad\times\{\mathrm{Re}[u^*_{k'}(z)]\cos(k'_zz+\alpha') + \mathrm{Im}[u^*_{k'}(z)]\sin(k'_zz+\alpha')\}\,dz. \end{aligned} \tag{A3}$$

In the limit $k'_z \to k_z$, i.e., $\Delta k_z = k_z - k'_z \to 0$, one has $\alpha' \to \alpha, u_{k'}(z) \to u_k(z)$, so $\mathrm{Re}[u^*_{k'}(z)] = \mathrm{Re}[u_k(z)]$ and $\mathrm{Im}[u^*_{k'}(z)] = -\mathrm{Im}[u_k(z)]$ and using the periodicity of $u_k(z)$ the integration in (A3) reduces to explicit integration in a single period of the SL. By further expanding of obtained expression through the use of asympthotic forms[41] of individual terms in it, after some algebra Eq. (A3) becomes

$$\begin{aligned} I = \frac{|K_e|^2}{d}\int_{\delta}^{\delta+d}\Bigg\{ &|u_k(\tilde z)|^2\pi\,\delta(\Delta k_z) + 2\,\mathrm{Re}[u_k(\tilde z)]\,\mathrm{Im}[u_k(\tilde z)]\,\mathcal{P}\left(\frac{1}{2k_z}\right)\cos(2k_z\tilde z + 2\alpha) \\ &-(\{\mathrm{Re}[u_k(\tilde z)]\}^2 - \{\mathrm{Im}[u_k(\tilde z)]\}^2)\,\mathcal{P}\left(\frac{1}{2k_z}\right)\cos(2k_z\tilde z + 2\alpha)\Bigg\}\,d\tilde z, \end{aligned} \tag{A4}$$

where $\tilde z = z - (l-1)d (\delta \le \tilde z \le \delta + d)$ and $\mathcal{P}(\frac{1}{2k_z})$ denotes the principal value. The last two terms in (A4) give finite values upon integration and may be neglected in comparison to the first term with $\delta(k_z - k'_z)$. From this first term and Eq. (A2) we find the normalization constant of even-parity continuum states, and normalized wave functions, Eq. (4). The normalized wave functions of odd-parity continuum states (5) are obtained in the same manner.

For bound-state wave functions, using Eqs. (16) and (17), and the normalization condition $\int_0^{+\infty}|\Psi_{\mathrm{bnd}}(z)|^2dz = 1/2$, we have

$$\int_0^{\delta} B^2_{e,o}y^2_{e,o}(z)dz + I_2 = \frac{1}{2}, \tag{A5}$$

where

$$\begin{aligned} I_2 &= C^2_{e,o}\sum_{l=1}^{+\infty}\int_{\delta+(l-1)d}^{\delta+ld}\{f_e[z-(l-1)d] + \theta_{\mathrm{bnd}}f_o[z-(l-1)d]\}^2e^{-2k_Id(l-1)}\,dz \\ &= C^2_{e,o}\sum_{l=1}^{+\infty}e^{-2k_Id(l-1)}\left[\int_{\delta}^{\delta+d}f^2_e(\tilde z)d\tilde z + \theta^2_{\mathrm{bnd}}\int_{\delta}^{\delta+d}f^2_o(\tilde z)d\tilde z + 2\theta_{\mathrm{bnd}}\int_{\delta}^{\delta+d}f_e(\tilde z)f_o(\tilde z)d\tilde z\right]. \end{aligned} \tag{A6}$$

The last term in (A6), integrating an odd function over full period, equals zero. Equation (A6) is actually a geometrical series, evaluation of which gives

$$I_2 = \frac{C_{e,o}^2 \int_{\delta}^{\delta+d} [f_e^2(z) + \theta_{\rm bnd}^2 f_o^2(z)] dz}{1 - e^{-2k_I d}}. \quad \text{(A7)}$$

The continuity of $\Psi_{\rm bnd}(z)$ at $z = \delta$, using Eqs.(16) and (17) gives

$$B_{e,o} = \frac{A_{e,o}}{y_{e,o}(\delta)} [f_e(\delta) + \theta_{\rm bnd} f_o(\delta)]. \quad \text{(A8)}$$

Substituting Eqs. (A7) and (A8) into (A5) we find the normalization constant of bound-states wave functions, Eq. (19).

In the special case of Kronig-Penney potential the normalization constants for both the continuum and bound states are straightforwardly derived using the fundamental solutions (23) and (24).

* Electronic address: indjin@kiklop.etf.bg.ac.yu

[1] L. Esaki and R. Tsu, IBM J. Res. Dev. **14**, 61 (1970).
[2] G. Bastard, *Wave Mechanics Applied to Semiconductor-Heterostructure* (Les Editions de Physique, Les Ulis, France, 1990).
[3] I. Tamm, Phys. Z. Sowjetunion **1**, 733 (1932).
[4] H. Ohno, E. E. Mendez, J. A. Brum, J. M. Hong, F. Agulló-Reneda, L. L. Chang, and L. Esaki, Phys. Rev. Lett. **64**, 2555 (1990).
[5] V. Milanović, Physica (Amsterdam) **121B**, 181 (1983).
[6] F. Y. Huang, Appl. Phys. Lett. **57**, 1669 (1990).
[7] M. Stęślicka, R. Kucharczyk, and M. L. Glasser, Phys. Rev. B **42**, 1458 (1990).
[8] S. G. Tikhodeev, Solid State Commun. **78**, 339 (1991).
[9] W. L. Bloss, Phys. Rev. B **44**, 8035 (1991).
[10] H. K. Sy and T. C. Chua, Phys. Rev. B **48**, 7930 (1993).
[11] W. Glessner and R. H. Yu, J. Appl. Phys. **73**, 4070 (1993).
[12] M. Stęślicka, R. Kucharczyk, L. Dobrzynski, B. Djafri-Rouhani, L. H. El Boudonti, and W. Jaskólski, Prog. Surf. Sci. **46**, 219 (1994).
[13] R. H. Yu, Appl. Phys. Lett. **65**, 1531 (1994).
[14] G. N. Henderson, L. C. West, T. K. Gaylord, C. W. Roberts, E. N. Glytsis, and M. T. Asom, Appl. Phys. Lett. **62**, 1432 (1993).
[15] L. C. West, C. W. Roberts, J. Dunkel, M. T. Asom, G. N. Henderson, T. K. Gaylord, E. Anemogiannis, and E. N. Glytsiss, *Quantum Well Intersubband Transitions Physics and Devices* (Kluwer, Dordrecht, 1994), pp. 511–524.
[16] M. Combescot and C. Benoit a la Guillaume, Solid State Commun. **39**, 651 (1981).
[17] G. Bastard, Phys. Rev. B **25**, 7584 (1982).
[18] A. Yariv and D. Yeh, *Optical Waves in Crystals* (John Wiley & Sons, New York, 1984).
[19] G. Lenz and J. Salzman, Appl. Phys. Lett. **56**, 871 (1990).
[20] F. Capasso, C. Sirtori, J. Faist, D. Sivco, S. N. G. Chy, and A. Y. Cho, Nature **358**, 565 (1992); C. Sirtori, F. Capasso, J. Faist, D. Sivco, S. N. G. Chy, and A. Y. Cho, Appl. Phys. Lett. **61**, 898 (1992).
[21] C. Sirtori, F. Capasso, J. Faist, D. Sivco, and A. Y. Cho, *Quantum Well Intersubband Transition Physics and Devices* (Ref. 15), pp. 301–311.
[22] C. Sirtori, F. Capasso, J. Faist, and S. Scandolo, Phys. Rev. B **50**, 8663 (1994).
[23] M. Zahler, E. Cohen, J. Salzman, E. Linder, and E. Maayan, Phys. Rev. B **50**, 5305 (1994).
[24] T. A. Weber, Solid State Commun. **90**, 713 (1994).
[25] R. A. Suris and P. Lavallard, Phys. Rev. B **50**, 8875 (1994).
[26] J. von Neumann and E. Wigner, Phys. Z. **30**, 465 (1929).
[27] F. H. Stillinger and D. R. Herrick, Phys. Rev. A **11**, 446 (1974).
[28] F. H. Stillinger, Physica (Amsterdam) **85B**, 270 (1977).
[29] G. Barton, J. Phys. A **18**, 779 (1985).
[30] H. Jones, *Theory of Brillouin Zones and Electronic States in Crystals* (North-Holland, Amsterdam, 1960).
[31] V. Milanović and D. Tjapkin, Phys. Status Solidi B **110**, 687 (1982).
[32] A. M. Kriman, N. C. Kluksdahl, and D. K. Ferry, Phys. Rev. B **36**, 53 (1987).
[33] Z. Ikonić, V. Milanović, and D. Tjapkin, Phys. Rev. B **32**, 8197 (1985).
[34] A. Sasaki, Phys. Rev. B **30**, 7016 (1984).
[35] V. Milanović and Z. Ikonić, Phys. Rev. B **37**, 7125 (1988).
[36] M. Tadić, V. Milanović, and Z. Ikonić, Phys. Rev. B **47**, 10 415 (1993).
[37] D. F. Nelson, C. M. Miller, and D. A. Kleinman, Phys. Rev. B **35**, 7770 (1987).
[38] *Intrisic Properties of Group IV Elements and III-V, II-VI and I-VII Compounds*, edited by K.-H. Hellwege and O. Madelung, Landolt-Börnstein, New Series, Group 3, Vol. 22, Pt. a (Springer-Verlag, Berlin, 1987).
[39] D. Campi, M. Meliga, and A. Pisoni, IEEE J. Quantum Electron. **30**, 2001 (1994).
[40] G. Henderson, T. K Gaylord, and E. N. Glytsis, Phys. Rev B **45**, 8404 (1992).
[41] A. Messiah, *Quantum Mechanics Vol. I* (North-Holland, Amsterdam, 1962).

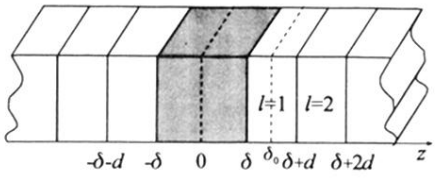

FIG. 1. A schematic representation of a periodic structure with a symmetric perturbation layer centered at the coordinate origin.

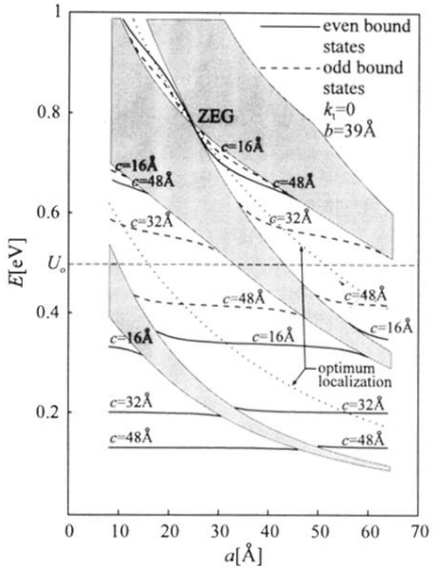

FIG. 3. The miniband structure of (AlIn)As/(GaIn)As superlattice with a perturbation layer, as it depends on the width of well-type layers a, for a couple of values of perturbation layer width c, and for the barrier layers width $b = 39$ Å (at $k_t = 0$). The allowed minibands are shaded, the even-parity bound states are represented by solid lines, and odd-parity ones by dashed lines. Dotted lines denote the position of bound states which would be optimal in respect to the degree of their localization.

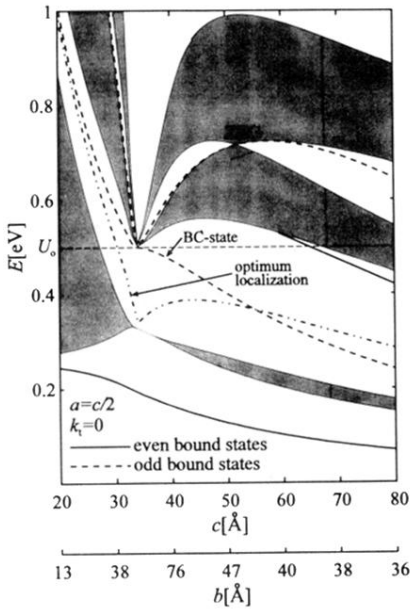

FIG. 4. The miniband structure of (AlIn)As/(GaIn)As Bragg-confined structure, as it depends on the perturbation layer width c. The width of barrier layers b was fitted to meet Bragg conditions for the odd-parity bound state in the first minigap (BC state) and is given on the bottom horizontal axis. The shaded areas denote the allowed minibands.

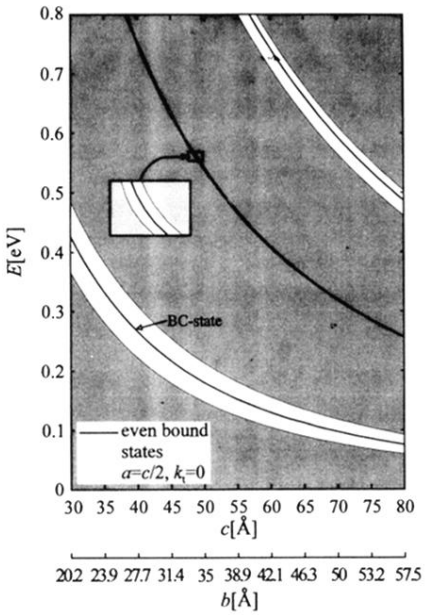

FIG. 5. The miniband structure of (InGa)As/InP effective mass Bragg-confined structure, as it depends on the perturbation layer width c. The width of barrier layers b was fitted to meet Bragg conditions for the even-parity bound state in the first minigap (BC state) and is given on the bottom horizontal axis. The shaded areas denote the allowed minibands.

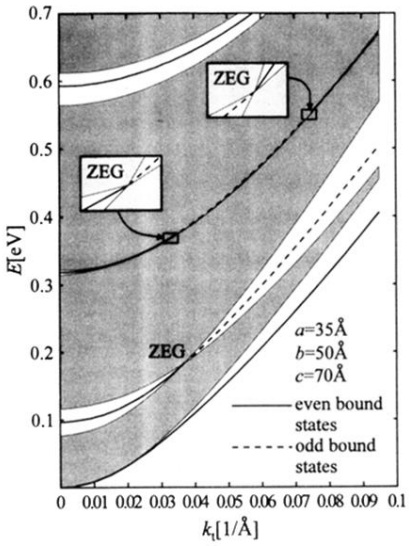

FIG. 6. The miniband structure of (InGa)As/InP effective-mass Bragg-confined structure, as it depends on the transverse wave vector k_t, calculated for a single set of the structure parameters. The shaded areas denote the allowed minibands.

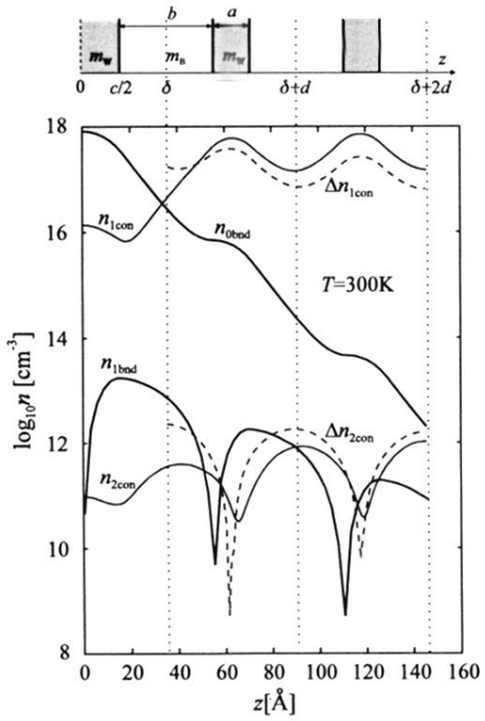

FIG. 7. The electron density profiles for the lowest two minibands ($n_{1\,\mathrm{con}}, n_{2\,\mathrm{con}}$) and the lowest two bound states ($n_{0\,\mathrm{bnd}}, n_{1\,\mathrm{bnd}}$) in (AlIn)As/(GaIn)As Bragg-confined structure. Also given (dashed lines) are the difference densities ($\Delta n_{1\,\mathrm{con}}, \Delta n_{2\,\mathrm{con}}$), referenced to the perfect superlattice case. The structure parameters are $c = 32$ Å, $a = 16$ Å, $b = 39$ Å.

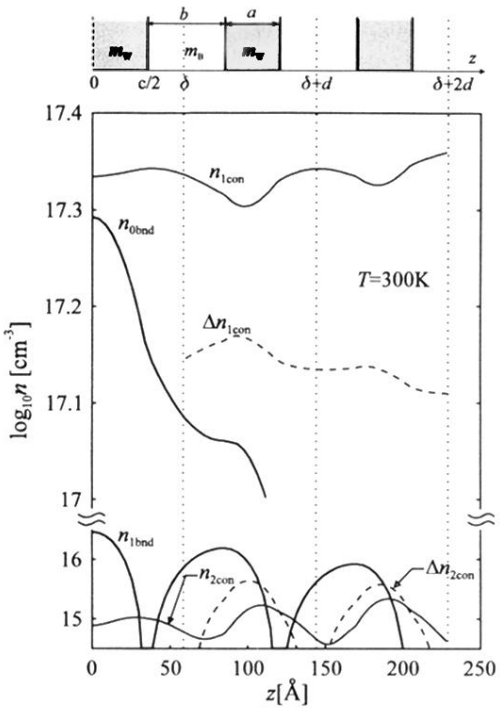

FIG. 8. The electron density profiles for the lowest two minibands ($n_{1\,\mathrm{con}}, n_{2\,\mathrm{con}}$) and the lowest two bound states ($n_{0\,\mathrm{bnd}}, n_{1\,\mathrm{bnd}}$) in (InGa)As/InP effective-mass Bragg-confined structure. Also given (dashed lines) are the difference densities ($\Delta n_{1\,\mathrm{con}}, \Delta n_{2\,\mathrm{con}}$), referenced to the perfect superlattice case. The structure parameters are $c = 70$ Å, $a = 35$ Å, $b = 50$ Å.